Heterogeneity and Persistence Length in Human Ocular Mucins

A. N. Round,* M. Berry,† T. J. McMaster,* S. Stoll,‡ D. Gowers,§ A. P. Corfield,† and M. J. Miles*

*H. H. Wills Physics Laboratory, University of Bristol, Bristol BS8 1TL, †Mucin Research Group, Bristol Eye Hospital, University of Bristol, Bristol BS1 2LX, and §School of Medical Sciences, Department of Biochemistry, University of Bristol, Bristol BS8 1TD, United Kingdom; and ‡Department of Inorganic, Analytical and Applied Chemistry, University of Geneva, CH-1211 Geneva 4, Switzerland

ABSTRACT Atomic force microscopy (AFM) has been used to investigate the heterogeneity and flexibility of human ocular mucins and their subunits. We have paid particular attention, in terms of theory and experiment, to the problem of inducing the polymers to assume equilibrium conformations at a surface. Mucins deposited from a buffer containing Ni^{2+} ions adopt extended conformations on mica akin to those observed for DNA under similar conditions. The heterogeneity of the intracellular native mucins is evident from a histogram of contour lengths, reflecting, in part, the diversity of mucin gene products expressed. Reduction of the native mucin with dithiothreitol, thereby breaking the S═S bonds between cysteine residues, causes a marked reduction in polymer length. These results reflect the modes of transport and assembly of newly synthesized mucins in vivo. By modifying the worm-like chain model for applicability to two dimensions, we have confirmed that under the conditions employed mucin adsorbs to mica in an equilibrated conformation. The determined persistence length of the native mucin, 36 nm, is consistent with that of an extended, flexible polymer; such characteristics will influence the properties of the gels formed in vivo.

INTRODUCTION

Mucins are a major component of the mucosal layer protecting passageways and surfaces that are exposed to foreign bodies in animals (Carlstedt and Davies, 1997), be they food, as in the case of the gastrointestinal mucins, or the atmosphere as exemplified by the respiratory, pulmonary, and ocular mucins. Ocular mucins are secreted by conjunctival goblet cells and epithelial cells of the ocular surface and by the lachrymal glands. They are present in the precorneal tear film, an aqueous gel layer critical to optical quality, transparency, and defense against the external environment (Corfield et al., 1997). Mucins possess physical and biological characteristics that reflect the physiological roles they perform: physically, mucins act as lubricants and form a physical protective barrier; biologically, they act as a matrix for smaller molecules and provide structures that bind microorganisms and immune cells both specifically and nonspecifically. For example, salivary mucins bind and aggregate a wide range of bacteria, suggesting that a generalist mechanism is employed (Groenink et al., 1997; Amerongen et al., 1995; Liu et al., 1999). Ocular mucus inhibits the adherence of microorganisms to the cornea, often to the extent that ocular surfaces are culture-negative for bacteria (Fleiszig et al., 1994).

Structurally, mucins are glycoconjugates, composed of polypeptide backbones encoded by members of the MUC gene family and decorated with O-linked oligosaccharide side chains. The four mucin genes believed to code for oligomeric gel-forming mucins (MUC2, MUC5AC, MUC5B, and MUC6) share the same basic layout of a variable number of tandem repeats that code for peptide sequences rich in proline, threonine, and serine (the latter two being potential sites of glycosylation), flanked by nonrepeating sequences containing cysteine-rich protein domains (Dusseyn et al., 2000). The length and composition of the tandem repeat varies between genes: for MUC2 it is 23 amino acids (aa) long, for MUC5AC it is 8 aa. Thus, a subunit is formed consisting of a linear proline, serine, and threonine-rich polypeptide between two globular, cysteine-rich domains. Assembly of these subunits via cysteine-cysteine bonds and glycosylation of the linear peptide sequences then forms the native mucin. The tear film contains mucins produced by at least four of the MUC genes: MUC1, MUC2, MUC4, and MUC5AC (Ellingham et al., 1999; Berry et al., 2000) produced by the ocular surface. MUC4 has also been isolated from the lachrymal gland (Berry et al., 2000). MUC1 mucin products are ubiquitous in the membranes of mucosal epithelia, MUC2 and MUC5AC produce secreted mucins, and the mucin produced by MUC4 has both membrane and secretory potential. The degree and nature of glycosylation depend on the origin (and function) of the mucin; ocular mucins possess short oligosaccharide side chains in comparison with many gastrointestinal mucins, yet typically carbohydrates account for 60–80% dry weight of these mucins. Charge, always negative, is conferred upon the polymer by sialic acids and sulfate groups within these side chains (Hazlett et al., 1986; Ellingham et al., 1999). As well as the binding functionality provided by the biochemically-specific moieties they contain, the oligosaccharide might impart a steric stiffness to the polypeptide core.

Physical characterization studies emphasize the polydispersity of the mucins, whether analyzed as tissue extracts (Berry et al., 1996) or single gene products (Sheehan et al.,

Submitted September 14, 2001, and accepted for publication April 8, 2002.

Address reprint requests to Dr. A. N. Round, H. H. Wills Physics Laboratory, Tyndall Avenue, Bristol BS8 1TL, UK. Tel.: 44-117-928-8743; 44-117-925-5624; E-mail: andy.round@bristol.ac.uk.

0006-3495/02/09/1661/10 $2.00

2000). Ocular mucins isolated from human conjunctiva and analyzed by size exclusion chromatography were found to have molecular masses in the range 2×10^3 to 2×10^6 kDa (Berry et al., 1996), and a similar range was found for mucins partially reduced by treatment with dithiothreitol (DTT). This heterogeneity is accounted for by the number of tandem repeats found within a subunit and the number of subunits assembled to form the whole, or native, mucin.

The inherent stiffness of a biopolymer is an important characteristic to consider, not only with regard to its behavior in solution, but also in the context of its synthesis and transport within the cell. This is illustrated by the packing of DNA within the chromosome, the transport of plant and bacterial structural polysaccharides to the cell wall (Carpita and Gibeaut, 1993), the storage of spider silk proteins before spinning (Vollrath and Knight, 2001), and the close packaging of mucins in secretory granules. The stiffness of the constituent polymers of a mucous gel will also have a direct influence on the structure of the gel, particularly on characteristics such as rheology, film stability, and pore size. Thus, the stiffness of these polymers, such as is estimated by the persistence length, is a useful property to measure with regard to the physiological role of mucin. A biopolymer's solution properties can be effectively simulated by the worm-like chain model (Kratky and Porod, 1949) and expressed in terms of stiffness or resistance to bending by the persistence length, *p*.

We have used atomic force microscopy (AFM) to assess how the properties of the tear film are related to the physical and biological properties of its constituent mucin polymers. AFM has proved to be a useful tool with which to explore biopolymer characteristics, often in biomimetic environments (Hansma, 2001). An advantage of AFM analysis over other techniques commonly used in this field (such as light scattering) is that it can be conducted at the level of individual molecules rather than relying on sampling a large population and producing an average result and is thus ideally suited to characterizing heterogeneous samples, including mucins and other complex biopolymers (McMaster et al., 1999; Round et al., 2001). Heterogeneity of polymers can be assessed from AFM images by constructing histograms of contour lengths of individual molecules. A number of recent studies have shown that AFM images can be used to calculate the persistence lengths of various polymers if the molecules are imaged in an equilibrium conformation (Rivetti et al., 1996; Balnois et al., 2000).

We have investigated a range of preparation methods for human ocular mucins to allow the polymers to reach equilibrium conformations at the mica surface. We have considered, in terms of the worm-like chain model, the effect of restricting a polymer to two dimensions. Using these methods, we have investigated the heterogeneity and flexibility of native and reduced ocular mucins and compared the results to those obtained for two plasmid DNA fragments of different lengths.

THEORY OF THE WORM-LIKE CHAIN MODEL

Polymers that appear to possess an inherent stiffness can be modeled by the Kratky-Porod, or worm-like, chain (Flory, 1969). This model was developed out of the freely rotating chain but introduces the notion of a continuously curved chain morphology where the angle between two segments (or unit vectors tangent to the segments) a distance ℓ apart along the chain (where $\ell \ll L$, the total length of the chain) is $\theta(\ell)$. For both the freely rotating and the worm-like chains in three dimensions the following relationships exist:

$$\langle \cos\, \theta(\ell) \rangle_{3D} = e^{-(\ell/p)} \tag{1}$$

and

$$\langle R^2 \rangle_{3D} = 2pL\left\{1 - \frac{p}{L}\left(1 - e^{(L/p)}\right)\right\}, \tag{2}$$

where p is the persistence length and $\langle R^2 \rangle$ is the mean-square end-to-end distance (for $L \rightarrow \infty$, $\langle R^2 \rangle_{3D} = 2pL$). This implicitly assumes that all angles $\theta(\ell)$ are independent of each other; i.e., it neglects larger-scale effects such as excluded volume. To model a polymer chain in two dimensions, Frontali et al. (1979) used a different concept of persistence length based on Schellman's hinge model (Schellman, 1974), where the chain is represented as a series of n links of equal length λ, whose equilibrium configuration is a rectilinear shape. The local change in free energy required to produce a bend through a two-dimensional angle $\theta(i)$ at the ith link is

$$\Delta g_i = \left(\frac{p'}{2\lambda k_B T}\right)\theta(i)^2_{2D}, \tag{3}$$

where p' is an expression of a local, microscopic resistance to bending and is directly comparable to the quantity p used in the worm-like chain model, providing large-scale effects such as excluded volume may be neglected. This being the case for polymers at concentrations low enough to avoid overlapping when deposited on mica (or equilibrium conformations in dilute solutions), the notation p will be used interchangeably hereafter. For a point j further along the chain, the curvilinear segment length $\ell = \lambda(j - i)$ can be substituted into Eq. 3, producing

$$\Delta g = \left(\frac{p}{2\ell k_B T}\right)\theta(\ell)^2_{2D} \tag{4}$$

As each link is independent of its neighbors, the probability density function of $\theta(\ell)$ is Gaussian, which has the follow-

ing consequences for its moments (averages of the *n*th powers of the deviation of $\theta(\ell)$ from the mean):

$$\langle \theta^{n=odd}(\ell)\rangle_{2D} = 0 \tag{5}$$

$$\langle \cos\,\theta(\ell)\rangle_{2D} = e^{-(\ell/2p)} \tag{6}$$

$$\langle \theta^2(\ell)\rangle_{2D} = \frac{\ell}{p} \tag{7}$$

$$\frac{\langle \theta^4(\ell)\rangle_{2D}}{\langle \theta^2(\ell)\rangle^2_{2D}} = 3 \tag{8}$$

Equations 6 and 7 thus give two straightforward ways of determining p whereas Eqs. 5 and 8 provide basic tests of whether a set of data has a Gaussian distribution. Equation 6 is also the direct two-dimensional equivalent of Eq. 1; the effect of removing a degree of freedom is manifest as a factor of ½ in the exponential term. Rivetti et al. (1996) considered a vector tangent to the chain at a given point in light of Eq. 6 and derived an expression for $\langle R^2\rangle_{2D}$ directly analogous to Eq. 2:

$$\langle R^2\rangle_{2D} = 4pL\left\{1 - \frac{2p}{L}\left(1 - e^{(L/2p)}\right)\right\} \tag{9}$$

Note that for $L \rightarrow \infty$, $\langle R^2\rangle_{2D} = 4pL$. This can be compared to the result of a simple projection of a three-dimensional chain on to the plane x, y:

$$\langle R^2\rangle_{proj} = \langle R_x^2\rangle + \langle R_y^2\rangle = \frac{2}{3}\langle R^2\rangle_{3D}, \tag{10}$$

where for $L \rightarrow \infty$, $\langle R^2\rangle_{proj.} = \frac{1}{3}\langle R^2\rangle_{2D}$. Measurement of this ratio can be used to determine whether the polymers are equilibrated or are trapped by the strength of their interaction with the mica surface.

MATERIALS AND METHODS

Mucin preparation

Mucins were extracted from human cadaver conjunctivae in 4 M guanidine hydrochloride (GuHCl) with protease inhibitors (Berry et al., 1996). Mature mucins were isolated on a cesium chloride gradient (buoyant density 1.35–1.45 g/ml) and confirmed free of DNA contamination (Hoechst 33258 dye). Samples were subsequently stored below 0°C in 0.5 M GuHCl and brought to ambient temperature before use. Native mucins were reduced with DTT by adding 20 μl 10 mM DTT in bicarbonate buffer to 200 μl of the mucin (diluted in deionized water) and standing for 1 h at room temperature or 24 h at 4°C.

DNA preparation

The two linear DNA fragments (2002 bp and 3145 bp) were obtained by digesting 5 μg of the plasmid pW149 (Wentzell and Halford, 1998) with the restriction enzyme pairs *Eco*RI/*Sap*I or *Eco*RI/*Psh*AI, respectively. Assuming a base-step size of 0.34 nm (Hagerman, 1981), this gives DNA fragments with chain lengths of 0.68 μm and 1.06 μm. The DNA fragments were separated on a 0.8% Tris acetate-EDTA agarose gel and purified using a Qiaex gel extraction kit, giving final concentrations of ~10 ng/μl (2.5 nM) in Tris-EDTA buffer. DNA was kept at 4°C and diluted (1:1 in 10 mM HEPES/2 mM $NiCl_2$) just before AFM measurements.

Atomic force microscopy

The microscope used in these experiments was a Multimode run from a Nanoscope IIIa controller (Digital Instruments/Veeco, Santa Barbara, CA). Olympus silicon cantilevers with a nominal spring constant of 42 Nm^{-1} were used for imaging in air whereas for working in liquid Nanoprobe silicon nitride cantilevers with a nominal spring constant of 0.38 Nm^{-1} were used.

Imaging in air

Native mucins were deposited in a variety of ways, as described in Results and Discussion. For the images used in the contour and persistence length calculations, the mucins and DNA were diluted in 10 mM HEPES/2 mM $NiCl_2$ and deposited onto mica in a 5-μl droplet, allowed to equilibrate for 60–300 s, rinsed in deionized water, and blown dry with nitrogen gas. Aminopropyltriethoxysilane (APTES) surfaces were prepared by the exposure of a freshly cleaved sheet of mica to APTES vapor in a desiccator for 2 h at room temperature. Mucins subjected to reduction with DTT (24 h) were treated in the same manner as above except that they were rinsed immediately after deposition.

Image analysis

The AFM images were reduced to binary images with ScionImage (Scion Corp., Frederick, MD; based on NIH Image), and the coordinates of each data point along the polymer chains were obtained using SigmaScan Pro (SPSS Science, Chicago, IL). The total contour length (L) and the distance between the two ends of each polymer (the end-to-end length, R) were then determined directly from these images.

The distribution of $\theta(\ell)$ was analyzed with a previously described program (Balnois et al., 2000). The program projects a series of segments of length ℓ onto a digitized polymer trace and measures the angles θ_k $\theta_{k+\ell}$, $\theta_{k+2\ell}$, etc. between vectors tangent to a segment at position k and at position $(k + \lambda)$, the angle $\theta_{k+\ell}$ between (vectors tangent to) segments $(k + \ell)$ and $(k + 2\ell)$ and so on along the length of the polymer up to $k + n\ell$. This process is repeated for segments separated by 2ℓ, 3ℓ, up to $n\ell$ so that values of $\langle \cos\,\theta(\ell)\rangle_{2D}$, $\langle \theta(\ell)\rangle_{2D}$, $\langle \theta^2(\ell)\rangle_{2D}$, and $\langle \theta^4(\ell)\rangle_{2D}/\langle \theta^2(\ell)\rangle^2{}_{2D}$ can be calculated.

RESULTS AND DISCUSSION

Adsorption of mucin to mica

To derive useful data from AFM images it is necessary to ensure that single polymers can be reproducibly imaged. Particular obstacles to this goal are the tendency of polymers to aggregate (as indeed, this is often their physiological function), either in solution or upon drying, and the electrostatic repulsion that occurs when anionic polymers interact with the negatively charged mica surface. Conformationally sensitive properties, such as the persistence length, require the polymers to assume equilibrium conformations before imaging. The inherent properties of the polymer should determine its conformation on a surface, not the properties of the surface. Many techniques have been

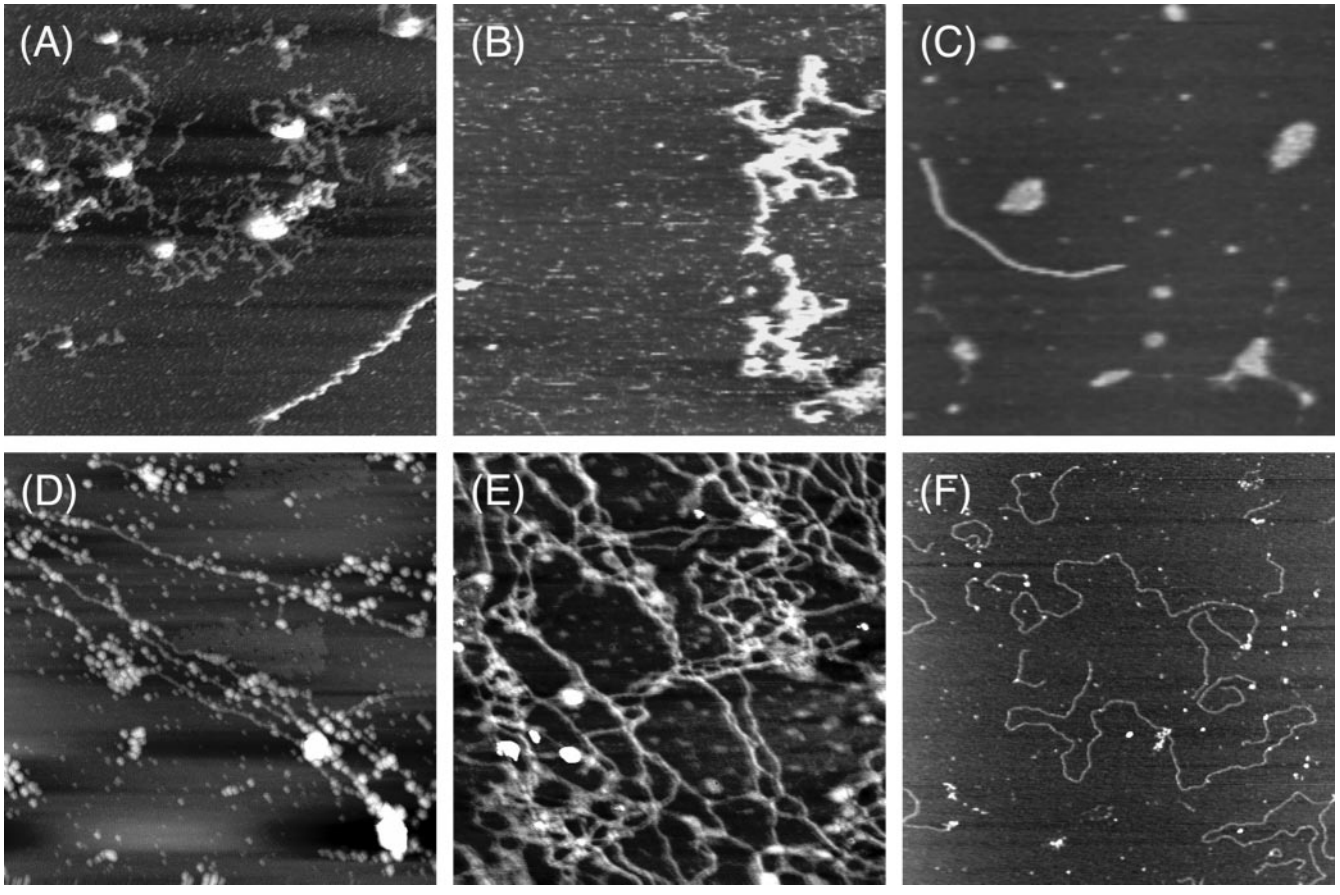

FIGURE 1 Images of native mucins obtained using a variety of preparation and deposition techniques: (*A*) droplet deposited and imaged in air (2 μm^2, 3 nm height); (*B*) droplet deposited and imaged in 10 mM Hepes/$NiCl_2$ (2 μm^2, 3 nm height); (*C*) spray deposited and imaged in air (2 μm^2, 5 nm height); (*D*) deposited by mica sandwich technique and imaged in air (2 μm^2, 4 nm height); (*E*) Ni-pretreated and imaged in air (2 μm^2, 2 nm height); (*F*) droplet deposited from 10 mM Hepes/2 mM $NiCl_2$ and imaged in air (2 μm^2, 2 nm height).

used to produce images of single polymers (Thundat et al., 1992; Schaper et al., 1994; Bezanilla et al., 1995; Mou et al., 1995; Hansma et al., 1997), but their applicability is often limited. Fig. 1 shows images of native mucins obtained using a variety of preparation and deposition techniques. Fig. 1 *A* shows mucin deposited from aqueous solution, dried, and imaged in air. The most common structures observed are compact aggregates with heights in excess of 3 nm, radiating from which are looped strands less than or equal to 1 nm in height. Given the expected dimensions of a polypeptide chain possessing short oligosaccharide side chains, these latter strands are interpreted as sections of individual mucin chains. The same sample, deposited as a droplet and dried, then imaged in a 10 mM HEPES, 2 mM $NiCl_2$ buffer produces images of which Fig. 1 *B* is typical. In comparison with Fig. 1 *A*, there are fewer compact aggregates and more extended linear structures. Most of these, however, are still more than 2 nm in height and therefore unlikely to be single polymers.

In an attempt to prevent the formation of aggregates, the same sample was deposited by spraying onto mica, following the technique of McIntire and Brant (1997). As Fig. 1 *C* shows, however, mucin deposited in this way forms compact, aggregated structures. Another method of disrupting aggregates is the so-called molecular combing, or mica sandwich, technique (Bensimon et al., 1995) shown in Fig. 1 *D*, whereby the sample drop is deposited on a mica sheet and spread by compression with a second sheet. The polymers are then aligned by shear flow as the droplet is compressed. This has the effect of producing linear features with heights of ~1 nm, consistent with the diameter of an ocular mucin. A large degree of association is still present, however, and the conformation of the polymers is clearly influenced by this deposition technique.

Hansma and Laney (1996) used divalent cations with a particular range of hydrated ionic radii and hydration enthalpies to form electrostatic bridges between DNA and mica and found that the DNA remained bound sufficiently strongly to allow reproducible imaging in buffer solutions. The structure of the basal plane of mica provides anionic pockets ~0.5 nm apart, so that availability of binding sites for the cation is not a limiting factor and does not affect the

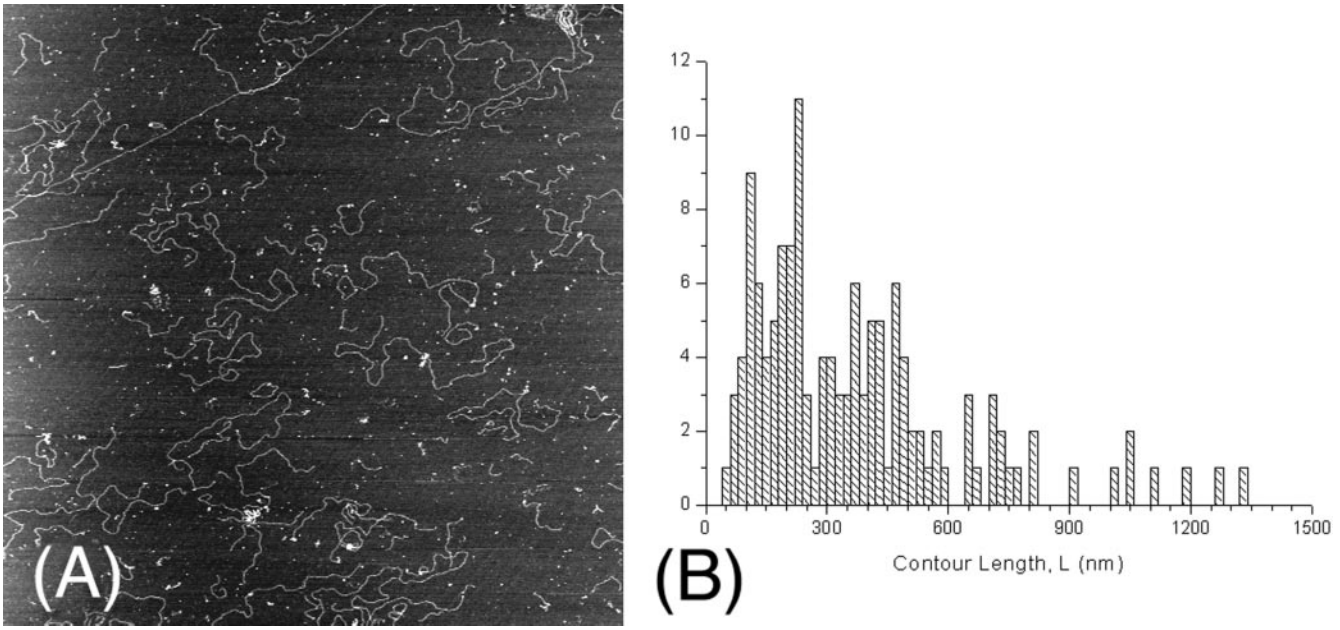

FIGURE 2 (*A*) Image (3 μm^2, 2 nm height) of native mucin; (*B*) Histogram of native mucin. In addition to the polymers measured here, many longer polymers were excluded as too long to capture entirely in one image. The heterogeneity of the protein backbone as well as that of the distribution of glycosylation makes it difficult to estimate an average molecular weight from AFM images.

conformation of the mucin. This electrostatic binding is also sufficiently weak to permit two-dimensional diffusion and the subsequent reaching of equilibrium by the polymer on the mica surface. Fig. 1 *E* shows the effect of pretreating mica with a solution containing divalent cations before deposition of the mucin solution, and it can be seen that images of 1–2-nm-high, extended linear polymers are produced. Images as shown in Fig. 1 *F* are produced when the mucin is diluted in HEPES/$NiCl_2$, deposited as a droplet onto unmodified mica, and imaged in air. These reproducibly show fields of individual extended polymers with an appearance similar to those seen in AFM images of DNA imaged under similar conditions (Rivetti et al., 1996). This observation agrees well with the characterization of cell-cultured and respiratory tract-secreted mucin polymers in solution as somewhat extended coils (Sheehan et al., 2000) and suggests that this method of immobilization is flexible enough to allow the inherent properties of the polymer to determine its final conformation on the surface. This technique was used in all images analyzed below.

Mucin heterogeneity

Of particular interest is the heterogeneity of the mucin population contained in the excluded fraction of a Sepharose CL2B size exclusion column (Fig. 2 *A*); individual polymers range in length from less than 100 nm to in excess of 3 μm. A histogram of native mucin lengths (Fig. 2 *B*) demonstrates this heterogeneity more clearly. This distribution under-represents the relative number and size of the larger mucins, because many long polymers extend beyond the edges of the image, and there exist some coiled and/or aggregated polymers of evidently great length. The heterogeneous nature of the glycosylation of the peptide backbone makes it difficult to estimate a meaningful value for a molecular weight from AFM images.

Images obtained in air after 24-h treatment with DTT show much shorter polymers, as a typical image demonstrates (Fig. 3 *A*). The corresponding length histogram (Fig. 3 *B*) shows that a large degree of heterogeneity remains and that some long polymers are still present after the reduction treatment; nevertheless, it is clear that the average polymer length is greatly reduced, and very long polymers (in excess of 3 μm) are absent. Fig. 3 *B* shows a major peak at 110 nm, suggesting that this is the length of a subunit or of a reduction-resistant mucin and is consistent with the length distribution of native mucin, which shows peaks at 110, 240, and 380–480 nm. The presence of peaks at lengths ~2, 3, and 4 times the major peak in the native mucin, and their subsequent absence from the DTT-treated fraction, allows the inference to be made that these longer polymers are di-, tri-, and tetramers of the 110-nm polymer.

Early dimerization and subsequent polymerization are part of the mucin biosynthetic pathway, and it has been suggested that the rheological properties of the mucus gel might be achieved by controlling mucin polymer length (Sheehan et al. 1995). The mode of aggregation for storage has not been elucidated yet. The presence of small molecules within the largest hydrodynamic volume fraction would suggest that some (disulfide) bonds between oli-

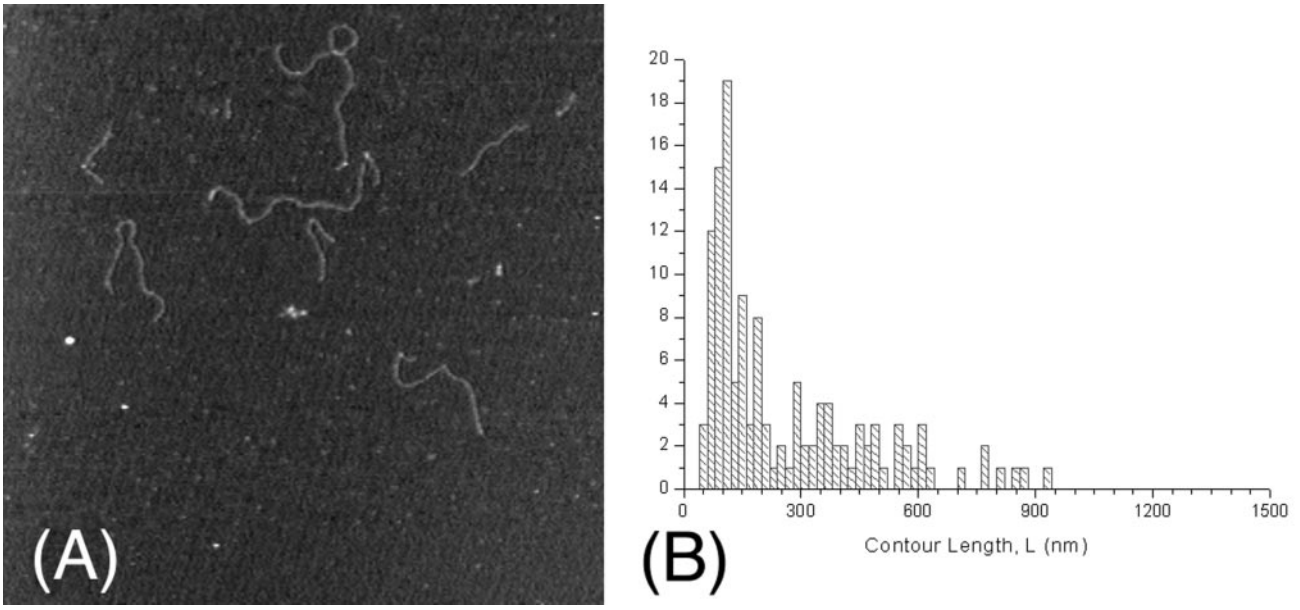

FIGURE 3 (*A*) Image (2.5 μm^2, 3 nm height) of reduced mucin; (*B*) Histogram of reduced mucin. Heterogeneity is markedly less in the reduced mucin fragments, and a periodicity reflecting the distribution of cysteine-rich regions is revealed based upon a 100-nm subunit, corresponding to ~40 tandem repeats of the MUC5AC gene product.

gomers are labile. Although these fragments may associate with longer (parent?) polymers during fractionation, the large dilution achieved for AFM visualization permits their detection. Secreted mucins are generally shorter than their intracellular counterparts due to intracellular processing or extracellular degradation processes. Cleavage sites within the C-terminal domain have been found in MUC2 (Herrmann et al., 1999) and MUC5B (Wickstrom et al., 1998), whereas a reduction in size was demonstrated for MUC5AC (Davies et al. 1999). A quantitative polymerase chain reaction study of the amounts of RNA transcripts corresponding to MUC2 and MUC5AC isolated from human conjunctiva (McKenzie et al., 2000) found that MUC2 transcripts were expressed at levels 5900-fold lower than MUC5AC transcripts, which may be interpreted as evidence that MUC5AC is the major DTT-labile mucin present and that the size decrease observed on treatment with DTT is predominantly due to the reduction of this mucin, although methylation of the MUC2 gene promoter would lead to an under-reporting of the amount present. If the cysteine-rich domains are fully reduced, then the major peak in the reduced mucin length histogram at 110 nm (Fig. 3 *B*) may correspond to a MUC5AC subunit consisting of ~40 tandem repeats.

The heterogeneity observed in this histogram reflects the presence of other mucin gene products, as well as variability in the number of tandem repeats in a subunit. In addition, some of the heterogeneity seen in the DTT-reduced samples may be due to the reassembly of subunits. Reassembly may be possible in the absence of a blocking agent and given the demonstrated surface mobility of mucin and other biopolymers in these conditions (McMaster et al., 1999; Gunning et al., 2000). Attempts to show the effect of using the blocking agent *N*-ethyl maleimide on reduced mucin lengths proved unsuccessful as the alkylated polymers formed small globular, rather than linear, structures (data not shown).

Polymer chain statistics

Rivetti et al. (1996) and Balnois et al. (2000) have shown that AFM images of DNA and succinoglycan, respectively, obtained in appropriate conditions, can be used to measure the persistence length. This model is valid only when polymers are imaged in a state of equilibrium; i.e., when $\langle\theta^4(\ell)\rangle/\langle\theta^2(\ell)\rangle^2 = 3$. Fig. 4 shows plots of this ratio versus inter-segment distances for the native mucin deposited from a solution containing Ni^{2+} cations (Fig. 4 *A*, as imaged in Fig. 1 *F*), mucin deposited using the mica sandwich technique (Bensimon et al., 1995) (Fig. 4 *B*, as imaged in Fig. 1 *D*), for plasmid DNA deposited from Ni^{2+} solution onto mica and allowed to equilibrate (Fig. 4 *C*), and for DNA deposited onto an APTES surface and immediately rinsed (Fig. 4 *D*). For inter-segment distances of ≤150 nm, this requirement is demonstrably satisfied in the cases of the DNA and the mucin deposited with Ni^{2+}. In the case of the mica-sandwiched mucins, the shear flow imparted during compression of the mica sheets has extended the mucins into nonequilibrium conformations, resulting in an average value of $\langle\theta^4(\ell)\rangle/\langle\theta^2(\ell)\rangle^2$ approaching 4 and also showing a significantly increased spread in the data, whereas for DNA deposited onto an APTES surface and not given time to

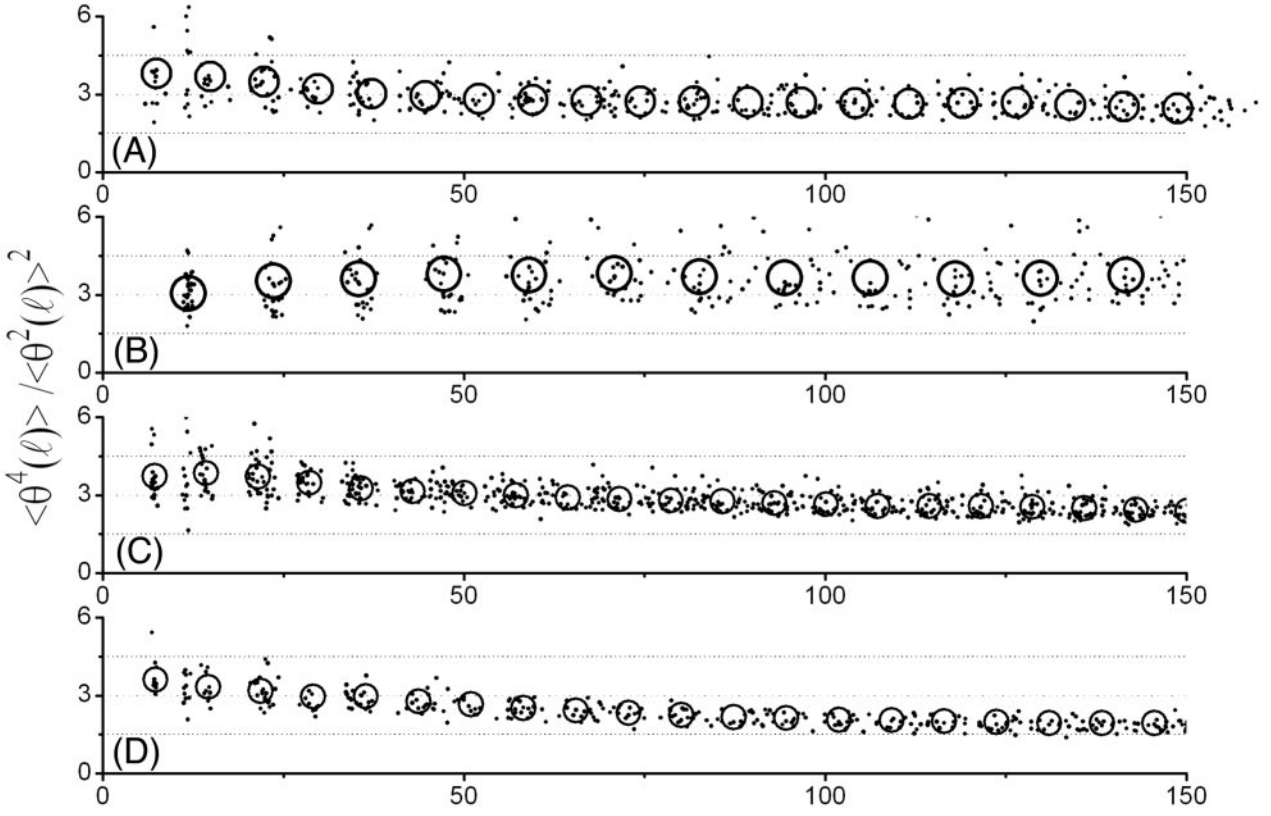

FIGURE 4 Plots of $\langle\theta^4(\ell)\rangle/\langle\langle\theta^2(\ell)\rangle^2$ versus segment separation (in nm): (*A*) mucin adsorbed onto mica; (*B*) mucin stretched by the mica sandwich technique; (*C*) DNA adsorbed onto mica; and (*D*) DNA deposited on an APTES-mica surface. Dots represent raw data, and open circles depict the average of all data in the plot (in each case n $\approx$ 50). The size of the open circles represents the standard deviation of the data for each series. The ratio $\langle\theta^4(\ell)\rangle/\langle\langle\theta^2(\ell)\rangle^2$ in graphs *A* and *C* remains close to 3, indicating that equilibrium is reached under these preparation conditions, whereas graphs *B* and *D* show the effects of preventing the polymers from occupying equilibrium conformations; in the case of stretched mucins the ratio approaches 4 whereas for DNA rapidly deposited on APTES-mica it drops to 2.

equilibrate, the ratio decreases to 2. It should also be noted that many of the shorter polymers more closely resemble rods than flexible chains. Plots of R^2/L versus L for native and reduced mucins and the two DNA fragments illustrate this clearly (Fig. 5). A large proportion of the reduced mucins (filled circles, Fig. 5 *A*) have lengths below 500 nm and a marked dependence of the ratio R^2/L on L, which is consistent with a plot of Eq. 9 (gray line). The large range of values for R^2/L (from 2 to 1000 nm for the other three systems studied) encompasses many different potential configurations, from straight rods to (almost) closed loops and is centered around a value close to $4pL$, in agreement with previous experimental data on single- and double-stranded xanthan (Stokke et al., 1986). This is also in line with expectations for a long Gaussian polymer, as demonstrated by the accompanying plots of Eq. 9 for each calculated persistence length. As the majority of polymers in the other three samples are sufficiently long to satisfy this criterion, the contour length of the polymer does not influence the measurement of the persistence length.

Having established the validity of the model for these systems, $\langle\theta^2(\ell)\rangle$ was plotted against ℓ (Fig. 6) and the persistence length p calculated using Eq. 7 (Table 1). Values of 56 $\pm$ 2 and 54 $\pm$ 2 nm are obtained for the 0.68- and 1.06-μm DNA samples, respectively, and a value of 36 $\pm$ 3 nm is calculated for the mucin sample. The DNA values are similar to those previously obtained from AFM images in these conditions (52 nm) (Rivetti et al., 1996) and those calculated from direct mechanical measurement (53 nm) (Bustamante et al., 1994). Calculated and directly measured values of the mean-square end-to-end distance in two dimensions and projected from three dimensions (Table 1) are close to those calculated for a Gaussian polymer equilibrated in two dimensions, providing further verification that these polymers are imaged at equilibrium. The mucin polymers obtained and purified from human ocular surfaces are therefore shown to be extended, flexible polymers.

Relating molecular properties to physiological roles

The properties of its constituent macromolecules will exert a strong influence on the properties of any supramolecular

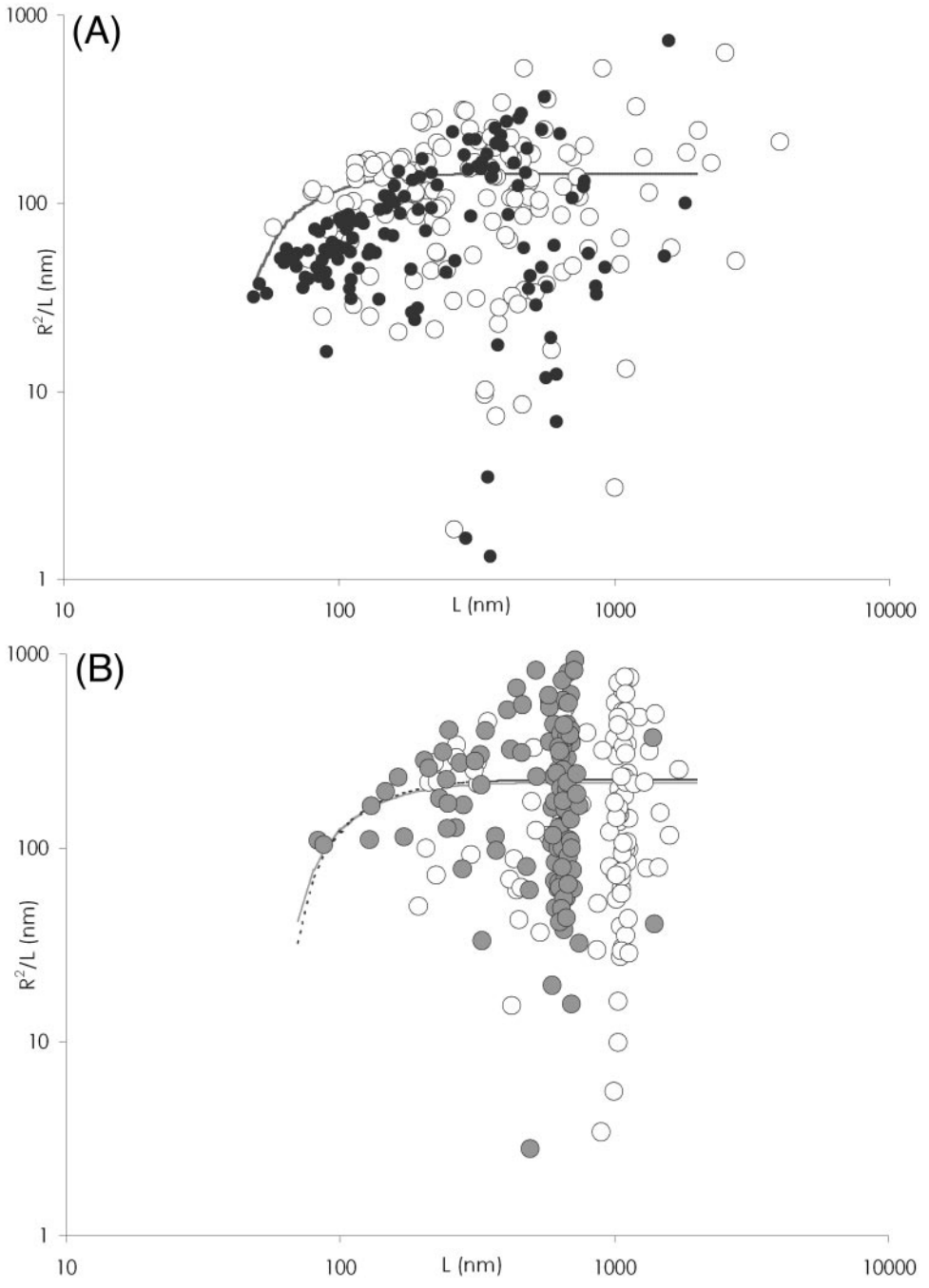

FIGURE 5 Log-log plots of R^2/L versus L: (*A*) native (*open circles*) and reduced (*filled circles*) mucin; (*B*) 0.68-μm plasmid DNA fragments (*shaded circles*) and 1.06-μm plasmid DNA fragments (*open circles*). The lines represent plots of Eq. 9 for the calculated persistence length of each polymer sample (in *b*, the broken dark line corresponds to the 0.68-μm plasmid DNA fragments, and the gray line to the 1.06-μm fragments). These plots demonstrate that for short polymers the persistence length is influenced by the contour length, but for longer polymers ($>10Lp$) no dependence exists.

structure. Ocular mucin polymers are believed to be responsible for tear film rheology and stability (Corfield et al., 1997). Mikkelsen et al. (1985) studied human bronchial mucins (collected from patients with chronic obstructive bronchitis, characterized by a persistent sputum gel) and found them to be highly flexible, random-coil macromolecules with a Kuhn length (which for a worm-like chain is twice the persistence length) of 2.5–3.5 nm, which could be readily distinguished from DNA in electron micrographs. Conversely, Sheehan et al. (2000) obtained the Mark-Houwink parameter α, an indicator of molecular stiffness in solution, for MUC5AC mucin and found it to be consistent

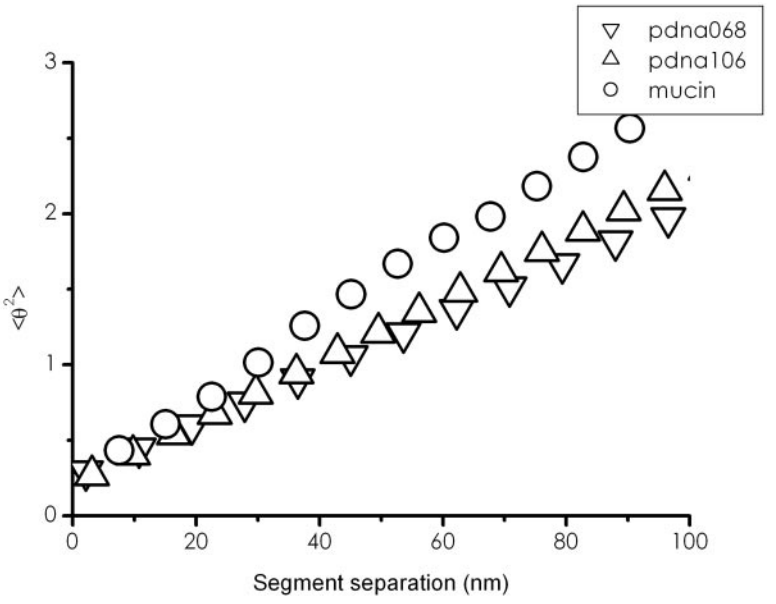

FIGURE 6 Plots of $\langle\theta^2\rangle$ versus segment separation for native mucin (○), 0.68-μm plasmid DNA fragments (▽); and 1.06-μm plasmid DNA fragments (△). The slopes of these curves gives the persistence lengths, which are 36 ± 3 nm for mucin and 54–56 ± 2 nm for the two DNA fragments.

with an extended, semi-flexible coil conformation, similar to that of DNA. The discrepancy between the values obtained for the MUC5AC products and those of, for example, Mikkelsen et al. (1985) and others were attributed to differences between a single gene product and mixtures of mucins normally present in mucosae. It is also possible that mucins produced from diseased tissue (as in the case of Mikkelsen's work) will have significantly different properties. Our results reveal that human ocular mucin that contains MUC5AC as well as other mucins behaves like the MUC5AC-containing samples. When imaged by AFM these mucins appear very similar to DNA in conformation (unlike the mucins of the obstructive bronchial mucus) and have a persistence length consistent with an extended semi-flexible polymer.

Conclusions

AFM images can provide information on the physical properties of biopolymers and the supramolecular structures they form. A modification of the worm-like chain model and comparison with images of DNA obtained under similar conditions confirmed that with simple, appropriate sample preparation mucin polymers reached equilibrium. Subsequent calculation revealed a persistence length for ocular mucins of 36 ± 3 nm. A subunit of 110 nm in length, consistent with a 40 tandem-repeat MUC5AC subunit, was a major component of the intracellular mucins. These data emphasize that MUC5AC is a major functional component of ocular mucins.

Mucosal gels, while maintaining a barrier for the penetration of foreign bodies, must also allow the diffusion of molecules between cell and surface. Both the contour and persistence lengths of the constituent polymers of the gel will influence the likely pore sizes in the gel and thus control the degree of diffusion permitted. The order of magnitude difference between pathological mucins forming tenacious gels and normal MUC5AC isolated in vivo and in vitro underlines the variation in mucin properties that are reflected in physiological function.

TABLE 1 Values of p for native mucin and the two plasmid DNA fragments and comparison of measured and calculated values of $\langle R^2\rangle$

	p ± SE (nm)	$\langle R^2\rangle_{\text{2D calc.}}$	$\langle R^2\rangle_{\text{proj.}}$	$\langle R^2\rangle_{\text{meas.}}$
Native mucin	36 ± 3	61,100	22,500	54,000
0.68-μm DNA	56 ± 2	94,300	34,300	101,000
1.06-μm DNA	54 ± 2	166,500	57,500	159,400

Values of $\langle R^2\rangle$ are rounded to the nearest 100 nm^2.

REFERENCES

Amerongen, A. V. N., J. G. M. Bolscher, and E. C. I. Veerman. 1995. Salivary mucins: protective functions in relation to their diversity. *Glycobiology.* 5:733–740.

Balnois, E., S. Stoll, K. J. Wilkinson, J. Buffle, M. Rinaudo, and M. Milas. 2000. Conformations of succinoglycan as observed by atomic force microscopy. *Macromolecules.* 33:7440–7447.

Bensimon, D., A. J. Simon, V. Croquette, and A. Bensimon. 1995. Stretching DNA with a receding meniscus: experiments and models. *Phys. Rev. Lett.* 76:4754–4757.

Berry, M., R. B. Ellingham, and A. P. Corfield. 1996. Polydispersity of normal human conjunctival mucins. *Invest. Ophthalmol. Vis. Sci.* 37: 2559–2571.

Berry, M., R. B. Ellingham, and A. P. Corfield. 2000. Membrane-associated mucins in normal human conjunctiva. *Invest. Ophthalmol. Vis. Sci.* 41:398–403.

Berry, M., T. J. McMaster, A. P. Corfield, and M. J. Miles. 2001. Exploring the molecular adhesion of ocular mucins. *Biomacromolecules.* 2:498–503.

Bezanilla, M., S. Manne, D. E. Laney, Y. L. Lyubchenko, and H. G. Hansma. 1995. Adsorption of DNA to mica, silylated mice, and minerals: characterization by atomic-force microscopy. *Langmuir*. 11: 655–659

Bustamante, C., J. F. Marko, E. D. Siggia, and S. Smith. 1994. Entropic elasticity of λ-phage DNA. *Science*. 265:1599–1600.

Carlstedt, I., and J. R. Davies. 1997. Glycoconjugates facing the outside world. *Biochem. Soc. Trans.* 25:214–219.

Carpita, N. C., and D. M. Gibeaut. 1993. Structural models of primary cell walls in flowering plants: consistency of molecular structure with the physical properties of the walls during growth. *Plant J.* 3:1–30.

Corfield, A. P., S. D. Carrington, S. J. Hicks, M. Berry, and R. Ellingham. 1997. Ocular mucins: purification, metabolism and functions. *Prog. Retin. Eye Res.* 16:627–656.

Davies, J. R., N. Svitacheva, L. Lannefors, R. Kornfalt, and I. Carlstedt. 1999. Identification of MUC5B, MUC5AC, and small amounts of MUC2 mucins in cystic fibrosis airway secretions. *Biochem. J.* 344: 321–330.

Dusseyn, J.-L., J.-P. Aubert, N. Porchet, and A. Laine. 2000. Evolution of large secreted gel-forming mucins. *Mol. Biol. Evol.* 17:1175–1184.

Ellingham, R. B., M. Berry, D. Stevenson, and A. P. Corfield. 1999. Secreted human conjunctival mucus contains MUC5AC glycoforms. *Glycobiology.* 9:1181–1189

Fleiszig, S. M. J., T. S. Zaidi, R. Ramphal, and G. B. Pier. 1994. Modulation of *Pseudomonas-aeruginosa* adherence to the corneal surface by mucus. *Infect. Immun.* 62:1799–1804.

Flory, P. J. 1969. Statistical Mechanics of Chain Molecules. Interscience, New York.

Frontali, C., E. Dore, A. Ferrauto, E. Gratton, A. Bettini, M. R. Pozzan, and E. Valdevit. 1979. An absolute method for the determination of the persistence length of native DNA from electron micrographs. *Biopolymers.* 18:1353–1373

Groenink, J., A. J. M.; Ligtenberg, A.-J. Van Winkelhoff, E. C. I. Veerman, and A. V. N. Amerongen,. 1997. XIV International Symposium on Glycoconjugates. Chapman and Hall, Zurich.

Gunning, A. P., A.R. Mackie, A. R. Kirby, P. Kroon, G. Williamson, and V. J. Morris. 2000. Motion of a cell wall polysaccharide observed by atomic force microscopy. *Macromolecules.* 33:5680–5685

Hagerman, P. J. 1981. Investigation of the flexibility of DNA using transient electric birefringence. *Biopolymers.* 20:1503–1535.

Hansma, H. G. 2001. Surface biology of DNA by atomic force microscopy. *Annu. Rev. Phys. Chem.* 52:71–92.

Hansma, H. G., K. J. Kim, D. E. Laney, R. A. Garcia, M. Argaman, M. J. Allen, and S. M. Parsons. 1997. Properties of biomolecules measured from atomic force microscopy images: a review. *J. Struct. Biol.* 119: 99–108.

Hansma, H. G., and D. E. Laney. 1996. DNA binding to mica correlates with cationic radius: assay by atomic force microscopy. *Biophys. J.* 70:1933–1939.

Hazlett, L. D., M. Moon, and R. S. Berk. 1986. In vivo identification of sialic-acid as the ocular receptor for *Pseudomonas-aeruginosa*. *Infect. Immun.* 51:687–689.

Herrmann, A., J. R. Davies, G. Lindel, S. Mårtensson, N. H. Packer, D. M. Swallow, and I. Carlstedt. 1999. Studies on the "insoluble" glycoprotein complex from human colon: identification of reduction-insensitive MUC2 oligomers and C-terminal cleavage. *J. Biol. Chem.* 274: 15828–15836.

Kratky, O., and G. Porod. 1949. Röntgenuntersuchung gelöszer Fadenmoleküle. *Rec. Trav. Chim. Pays-Bas*. 68:1106–1123.

Liu, B., S. Rayment, F. G. Oppenheim, and R. F. Troxler. 1999. Isolation of human salivary mucin MG2 by a novel method and characterization of its interactions with oral bacteria. *Arch. Biochem. Biophys.* 364: 286–293.

McIntire, T. M., and D. A. Brant. 1997. Imaging of individual biopolymers and supramolecular assemblies using noncontact atomic force microscopy. *Biopolymers.* 42:133–146.

McKenzie, R. W., J. E. Jumblatt, and M. M. Jumblatt. 2000. Quantification of MUC2 and MUC5AC transcripts in human conjunctiva. *Invest. Ophthalmol. Vis. Sci.* 41:703–708.

McMaster, T. J., M. Berry, A. P. Corfield, and M. J. Miles. 1999. Atomic force microscopy of the submolecular architecture of hydrated ocular mucins. *Biophys. J.* 77:533–541.

Mikkelsen, A., B. T. Stokke, B. E. Christensen, and A. Elgsaeter. 1985. Flexibility and length of human bronchial mucin studied using low-shear viscometry, birefringence relaxation analysis and electron microscopy. *Biopolymers.* 24:1683–1704.

Mou, J., D. M. Czajkowsky, Y. Zhang, and Z. Shao. 1995. High-resolution atomic force microscopy of DNA: the pitch of the double helix. *FEBS Lett.* 371:279–282.

Rivetti, C., M. Guthold, and C. Bustamante. 1996. Scanning force microscopy of DNA deposited onto mica: equilibration versus kinetic trapping studied by statistical polymer chain analysis. *J. Mol. Biol.* 264:919–932.

Round, A. N., N. M. Rigby, A. J. MacDougall, S. G. Ring, and V. J. Morris. 2001. Investigating the nature of branching in pectin by atomic force microscopy and carbohydrate analysis *Carb. Res.* 331:337–342

Schaper, A., J. P. P. Starink, and T. M. Jovin. 1994. The scanning force microscopy of DNA in air and in *n*-propanol using new spreading agents. *FEBS Lett.* 355:91–95.

Schellman, J. A. 1974. Flexibility of DNA. *Biopolymers.* 13:217–226.

Sheehan, J. K., C. Brazeau, S. Kutay, H. Pigeon, S. Kirkham, M. Howard, and D. J. Thornton. 2000. Physical characterization of the MUC5AC mucin: a highly oligomeric glycoprotein whether isolated from cell culture or in vivo from respiratory mucous secretions. *Biochem. J.* 347:37–44.

Sheehan, J. K., C. Hansk, A. P. Corfield, C. Paraskeva, and D. J. Thornton. 1995. Mucin biosynthesis and macromolecular assembly. *Biochem. Soc. Trans.* 23:819–821.

Stokke, B. T., A. Elgsaeter, and O. Smidsrød. 1986. Electron microscopic study of single- and double-stranded xanthan. *Int. J. Biol. Macromol.* 8:217–225.

Thundat, T., D. P. Allison, R. J. Warmack, G. M. Brown, K. B. Jacobson, J. J. Schrick, and T. L. Ferrell. 1992. Atomic force microscopy of DNA on mica and chemically modified mica. *Scan. Microsc.* 6:911–918.

Vollrath, F., and D. P. Knight. 2001. Liquid crystalline spinning of spider silk. *Nature.* 410:541–548

Wentzell, L. M., and S. E. Halford. 1998. DNA looping by the SfiI restriction endonuclease. *J. Mol. Biol.* 281:433–444.

Wickstrom, C., J. R. Davies, G. V. Eriksen, E. C. Veerman, and I. Carlstedt. 1998. MUC5B is a major gel-forming, oligomeric mucin from human salivary gland, respiratory tract and endocervix: identification of glycoforms and C-terminal cleavage. *Biochem. J.* 334:685–693.